Cementation and structural diagenesis of fluvio-aeolian Rotliegend sandstones, northern England

Benjamin Busch[1,2]*, Christoph Hilgers[1,2], Lars Gronen[3] & Dirk Adelmann[4]

[1] Institute of Reservoir Petrology, EMR | Energy and Mineral Resources Group, RWTH Aachen University, Wuellnerstraße 2, Aachen 52062, Germany
[2] Present address: Department of Structural Geology and Tectonophysics, Institute of Applied Geosciences, Karlsruhe Institute of Technology, Adenauerring 20a, Karlsruhe 76131, Germany
[3] Institute for Applied Mineralogy and Economic Geology, EMR | Energy and Mineral Resources Group, RWTH Aachen University, Suesterfeldstraße 2, Aachen 52062, Germany
[4] Wintershall Holding GmbH, Friedrich Ebert Straße 160, Kassel 34119, Germany
   B.B., 0000 0002 3456 2592; C.H., 0000 0002 5194 4349; L.G., 0000 0002 9957 1262; D.A., 0000 0002 4973 8036
* Correspondence: benjamin.busch@kit.edu

Abstract: Quartz cementation in sandstones is closely linked to grain coating phases and diagenetic alteration. Grain coatings consisting of illite smectite stained with iron oxides and hydroxides are able to preserve large amounts of porosity by preventing the formation of syntaxial quartz overgrowth cement. The Penrith Sandstone Formation was chosen as an analogue for Rotliegend reservoirs to test the impact of grain coatings on quartz cementation. This adds to an existing model of cementation. Differences of grain coating coverage can be linked to grain size. Extensive grain coatings are present in finer grained laminae in some samples. Coarser grained laminae contain less extensive grain coatings. The analysis of grain coatings based on standard petrographic analyses is combined with high resolution QEMSCAN® analyses. Structural features include deformation bands of different ages. Diagenetic alterations around faults, recorded by grain coatings, allow the delineation of relative temporal relations, revealing at least two generations of deformation band formation associated with normal faulting. In the Vale of Eden succession one normal faulting event postdates burial diagenetic quartz cementation as is evident by fault focused fluid flow and associated bleaching of iron and absence of quartz overgrowth.

Cementation and chemical compaction are the two main factors controlling reservoir quality in deeply buried sandstone reservoirs (e.g. Paxton *et al.* 2002; Taylor *et al.* 2010, 2015). Reservoir quality is controlled by depositional and early diagenetic processes such as grain coatings inhibiting quartz overgrowth cementation (Ajdukiewicz *et al.* 2010; Taylor *et al.* 2010; Ajdukiewicz & Larese 2012). One of the depositional environments affected by grain coatings is aeolian dune deposits, which can preserve considerable amounts of porosity during diagenesis and deep burial (Ajdukiewicz *et al.* 2010). Additionally, reservoir quality can be influenced by structural compartmentalization by faulting and fault associated processes such as deformation bands (Antonellini & Aydin 1994; Fisher & Knipe 2001; Fossen & Bale 2007; Tueckmantel *et al.* 2012).

Authigenic grain coating phases consisting of clay minerals are reported to form from detrital precursor clay mineral phases deposited on grain surfaces during deposition and early diagenesis (Ajdukiewicz & Larese 2012). During burial diagenesis, these precursor minerals, commonly smectite, can transform to other clay minerals such as tangential or radial illite or chlorite (Aagaard *et al.* 2000; Worden & Morad 2002). An important factor for the emplacement of detrital clay minerals into the sediment body seems to be a periodical influence of meteoric waters during generally arid conditions (Salem *et al.* 2000; Esch *et al.* 2008; Ajdukiewicz *et al.* 2010). The climatic conditions and the supply of meteoric waters are therefore considered to have a major impact on early diagenetic clay mineral coat formation (Esch *et al.* 2008; Ajdukiewicz *et al.* 2010).

Deformation bands are zones of localized deformation found in granular media such as siliciclastic rocks and limestones (e.g. Antonellini & Aydin 1994, 1995; Fossen *et al.* 2007; Wennberg *et al.* 2013). The formation of deformation bands is linked to faulting processes, and they can form from consolidated and unconsolidated sandstones as precursors to or concurrent with fault localization (Fowles & Burley 1994; Antonellini & Aydin 1995; Rotevatn *et al.* 2007; Johansen & Fossen 2008). Deformation bands generally reduce permeability (Fossen & Bale 2007; Tueckmantel *et al.* 2012; Busch *et al.* 2017), but permeability may locally be enhanced parallel to the strike of the deformation bands (Fowles & Burley 1994). During fault focused fluid migration the fault's damage zone and the surrounding lithology can be altered, as is evident from colour alterations of faulted red bed sediments (Eichhubl *et al.* 2004; Parry *et al.* 2004; Eichhubl & Flodin 2005). This alteration can be used to infer the diagenetic history and to delineate fault related alteration of the host rock.

In this study, we present petrographic and structural geological data from aeolian Rotliegend rocks, where zones of preferential quartz cementation were previously reported (Arthurton & Wadge 1981; Turner *et al.* 1995). This lithology can be seen as analogous to some Northern European onshore and offshore plays. Notable areas are the Permian Central European Basin System and the East Irish Sea Basin. In the study area in the Vale of Eden the presence and extent of grain coatings was evaluated as a possible control on the volumes of syntaxial quartz overgrowth. We expand the previous model of cementation (Turner *et al.* 1995) and present a paragenetic sequence. The incorporation of diagenetic alterations surrounding normal faults and deformation bands allows the relative dating of deformation and diagenetic alteration. Additionally, we integrate QEMSCAN® analyses and standard petrographic analyses and test their applicability to the studied dataset on two selected samples.

Geological setting

The outcrops of Permian strata in the Vale of Eden half graben, Cumbria, UK, cover an area of *c.* 48 × 6 km (Macchi 1981; Turner *et al.* 1995) (Fig. 1a). Permian strata in the region are combined in the Appleby Group, consisting of the aeolian Penrith Sandstone Formation and basal alluvial deposits locally referred to as the Brockram facies (Arthurton & Wadge 1981; Macchi 1981; Hughes 2003). The Brockram facies interdigitates with the Eden Shales Formation deposited during the Zechstein in the southeastern part of the Vale of Eden around Kirkby Stephen (Macchi 1981). The lithologies dip gently towards the NE at 5° (Fig. 1b). The dip of the strata changes towards the Pennine Fault System to a dip of *c.* 20° towards the SW (Fig. 1b) (Arthurton & Wadge 1981). The Appleby Group unconformably overlies Upper Carboniferous siliciclastic rocks in the northern part of the Vale of Eden and Lower Carboniferous limestones in the south (Arthurton & Wadge 1981; Macchi 1981; Turner *et al.* 1995) (Fig. 1b). The Appleby Group is conformably overlain by the Zechstein deposits consisting of shales, evaporites and dolomite, which are combined in the Eden Shales Formation (Arthurton & Wadge 1981). The oldest part of the Eden Shales Formation is the Hilton Plant Beds, which consist of laminated, calcareous or dolomitic, fine grained sandstones (Hughes 2003). The Eden Shales Formation mainly consists of
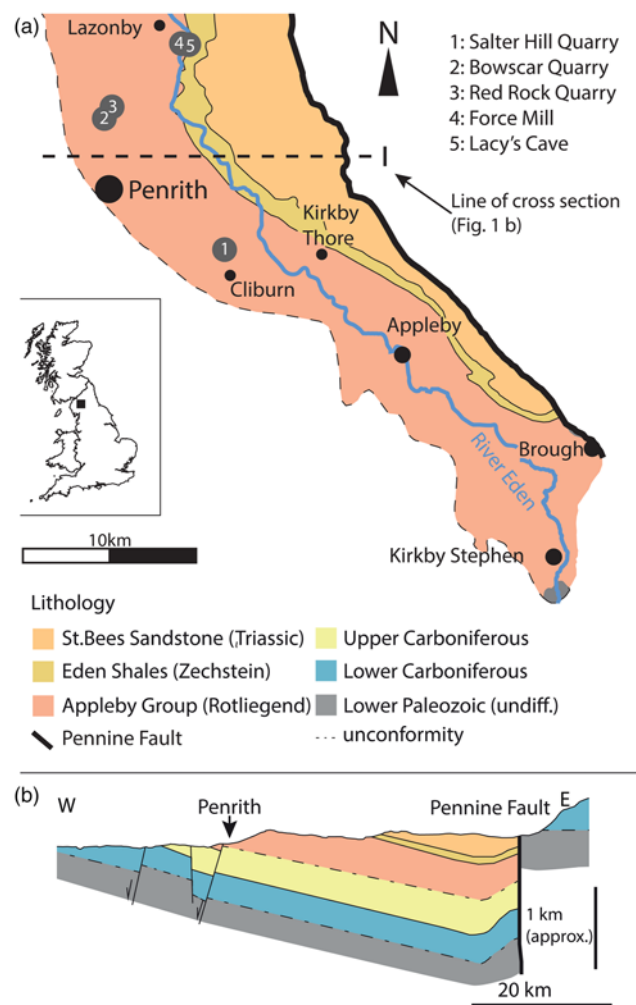

Fig. 1. (**a**) Overview of the study area in the Vale of Eden half-graben, Cumbria, UK. Locations of the five studied exposures are highlighted. Line of cross-section is indicated. (**b**) Schematic cross-section of the Vale of Eden half-graben north of Penrith. The Permo-Triassic units of the Vale of Eden dip gently towards the NE (redrawn and modified from Turner *et al.* (1995); vertical scale is given separately).

red and grey mudstones intercalated with carbonates and gypsum anhydrite evaporites (Beds A D) (Turner *et al.* 1995; Hughes 2003). The marine Belah Dolomite is a marker horizon present throughout the Vale of Eden and appears below the evaporitic D bed within the Eden Shales Formation (Hughes 2003). Triassic deposits in the region are present as the St Bees Sandstone of the Sherwood Sandstone Group (Hughes 2003). In the southeastern part of the Vale of Eden the Eden Shales Formation and Sherwood Sandstone Group are described as interdigitating with the Stenkrith Brockrams (Macchi 1981).

The presence of non silicified parts of the Penrith Sandstone Formation was reported to be restricted to the occurrence of the Brockrams, alluvial fan deposits composed of limestone breccias (Waugh 1970*b*). A gradual increase in quartz cement has been correlated with the thinning out of the Brockrams between Appleby, Cliburn and Kirkby Thore (Waugh 1970*b*). The lower parts of the succession near Cliburn appear unsilicified, whereas at Penrith almost the entire succession is silicified (Waugh 1970*b*).

Turner *et al.* (1995) proposed a model for the cementation of the Penrith Sandstone Formation, which links the localized quartz cementation to the dip of the formation during burial and the levelling of the palaeo water table. The saline, more quartz rich fluid phase accumulated below an unconformity, resulting in the localized abundance of quartz cement (Turner *et al.* 1995). The most likely source of silica was reported to be alkaline, saline fluids from the Upper Permian (Zechstein) Eden Shales Formation (Turner *et al.* 1995). Alkaline formation waters are able to support a higher saturation of silica in solution than the more acidic formation waters of Upper Carboniferous strata, which consist of sandstones, shales and coal seams (Pennine Coal Measures Group and Millstone Grit) (Turner *et al.* 1995). The source of the silica bearing solutions is additionally supported by saline fluid inclusions in quartz overgrowth cements measured in samples from the Penrith Sandstone Formation (Turner *et al.* 1995).

Structural development

The half graben is bounded by the Dent Fault Line to the south and the Pennine Fault System to the NE (Underhill *et al.* 1988; Fowles & Burley 1994) (Fig. 1a). The half graben formed during early Permian rifting and subsidence actively continued until the Cretaceous to a maximum depth of *c.* 3500 m (Turner *et al.* 1995). Reactivation and basin inversion from the late Cretaceous to the present uplifted the strata to their present position (Turner *et al.* 1995). The structural inventory also includes deformation bands associated with normal faulting (Fowles & Burley 1994; Guo *et al.* 2009).

The general timing of fault movement is unclear (Fowles & Burley 1994). However, the timing of the large scale Pennine Fault System and Dent Fault System is well constrained (Underhill *et al.* 1988; Turner *et al.* 1995). Relative dating of some structural elements is possible around the Armathwaite Cleveland Dyke. The Tertiary Armathwaite Cleveland Dyke (emplaced at 58.4 ± 1.1 Ma; MacDonald *et al.* 1988) is offset by NE SW to ENE WSW striking normal faults (Fowles & Burley 1994). The similar strike of deformation bands and larger scale faults indicates that they were formed contemporaneously within a similar stress field (e.g. Antonellini & Aydin 1995; Johansen & Fossen 2008; Fossen & Rotevatn 2012).

The NNW SSE striking faults most probably resemble a phase of formation during early subsidence controlled by the large Pennine Fault system (Underhill *et al.* 1988). This fault was active during the deposition of the Penrith Sandstone and during the Tertiary (Arthurton & Wadge 1981). Initiated during the Alpine orogeny, the down to the west faulting reactivated many older faults (Arthurton & Wadge 1981).

The NE SW striking faults can be related to a late phase of normal faulting also displacing the Armathwaite dyke (Fowles & Burley 1994). Additionally, the NE SW striking faults mostly abut against NNW SSE striking faults (Fowles & Burley 1994). This abutting relation supports a younger age for the NE SW striking faults (e.g. Nixon *et al.* 2014). Fowles & Burley (1994) pointed out the similar strike of the Dent Fault zone in the south. Arthurton & Wadge (1981), however, underlined the importance of basal normal faults separating the depositional environments of the Carlisle and Vale of Eden Basins in the north of the area.

A minor west east striking normal fault was mapped by Fowles & Burley (1994). The timing is not further constrained.

Both major faulting events present in the Vale of Eden are thought to be inherited from older strata (Arthurton & Wadge 1981).

Materials and methods

Oriented samples were collected from closed and active quarries (Red Rock Quarry, Bowscar Quarry, Salter Hill) (Fig. 1a). A few oriented samples were collected surrounding Lacy's caves and on the opposite bank of the River Eden at Force Mill (Fig. 1a). Cementation of the samples has mainly been studied on thin sections. The sampling sites were chosen because of the reported quartz cementation in the region (Waugh 1970*b*) and as analogues in terms of depositional environments (Mader & Yardley 1985) to other European Rotliegend deposits. Thin sections were stained with a blue dyed epoxy resin to visualize porosity and were prepared to be 30 μm thick. Point counting was performed with 300 counts on a grid (step length adjusted to maximum grain size) with a Pelcon Point Counter mounted on a Zeiss Axio Lab microscope and plotted according to Folk (1980). One occurrence of a mineral will result in a mineral quantity of 0.3%. Where a deformation band was included in the sample the modal contents were evaluated in the undisturbed host rock. General petrographic analysis was performed with a Leica DMLP microscope fitted with an Invenio 5DII camera controlled by DeltaPix Insight software. For each sample the coating coverage was evaluated based on 50 grains per sample. The coating coverage is the relative amount of grain surface covered by a grain coating phase that is in contact with the intergranular volume (IGV) (e.g. Taylor *et al.* 2004). Grain coatings present at grain contacts are omitted in this evaluation but yield information on a possible detrital origin of the grain coating phase. Grain sizes and sorting characteristics were derived from measurements of the long axis on at least 100 grains per sample on a grid adjusted to the maximum grain size to retrieve area weighted results.

Two polished thick sections (100 μm) were prepared and coated with carbon for QEMSCAN® analyses at the Institute for Applied Mineralogy and Economic Geology at RWTH Aachen University. Opposing pieces of samples BQ 2 and FM Alt have been prepared and are denoted by the suffix ' Q' in the sample name. QEMSCAN® analyses were applied to visualize the distribution of minerals within selected samples. QEMSCAN® is a semi automated mineralogical tool based on an SEM platform. Supported by fast acquisition energy dispersive X ray spectroscopy (EDX; DualXFlash SDD Brucker) and back scattered electron/secondary electron (BSE/SE) imaging detectors, QEMSCAN® has the advantage of scanning large sample surfaces at high resolutions. EDX spectra and BSE grey level intensities were recorded for each sampling point and combined to be assessable pixel information. This combination is used for phase or mineral interpretation by adjustable purpose built species interpret ation profiles (SIP). Pixels of the same phase sharing edges are handled as particles. Using image analysis, these particles are surveyed for geometrical (e.g. size, shape and associations) and chemical (elemental distribution and mapping) properties. Volumetric distributions of phases are gathered from the surface coverage of the specific phases to generate modal compositions.

Analyses of the carbon coated samples were performed with a Quanta 650 F QEMSCAN® (FEI) platform with a point spacing of 5 μm to obtain a reasonable file size while having a high resolution for sample BQ 2 Q. For the presented thin section sample 18 932 350 separate points on the sample surface have been analysed, excluding pores. Sample FM Alt Q was measured with a point spacing of 2 μm, and 4 750 959 points were acquired in the bleached part of the section and 4 540 022 points in the unbleached part, both excluding porosity. The electron beam was accelerated by 15 kV and the sample current was held at 10 nA, and both were automatically checked and adjusted over a 2 h cycle during the whole measurement. For each pixel EDX spectra were recorded until 2000 counts were gathered. The working distance (sample surface to pole piece) was set to 13 mm.

Results

Petrography

The aeolian samples from Bowscar Quarry, Red Rock Quarry, Salter Hill, Force Mill and Lacy's Cave feature average grain sizes from 0.15 to 0.47 mm (Table 1), and are moderately to moderately well sorted. Samples occasionally show bimodal laminations.

Detrital components were determined by point counting 15 thin sections, giving 60 78.7% quartz grains, 3 6.3% K feldspar grains, 0 0.3% plagioclase and 0.3 3.3% rock fragments (Table 1). The sandstones can be classified according to Folk (1980) as quartzarenites to subarkoses (Fig. 2). Quartz grains appear with a monocrystalline, polycrystalline or undulose extinction pattern.

Feldspars are often dissolved or altered and are replaced by either kaolinite or illite (Fig. 3b d). Skeletal frameworks of dissolved feldspars are commonly surrounded by the replacive mineral. Occasionally the feldspars are dissolved without any replacive phases in the vicinity. The pigmented hematite dust rim outlining the detrital grain boundaries is often preserved during alteration (Fig. 3b). Kaolinite appears in two types: type I kaolinite is unaltered and type II kaolinite is (partly) illitized, as could be observed in QEMSCAN® analyses and transmitted light micros copy (Fig. 3e and f). Most feldspars are at least slightly illitized. Detrital mineral grains include iron oxide grains, titanite, muscovite, tourmaline and zircon.

Prominent rock fragments include silicic and feldspar rich volcanic fragments, shale rock fragments, sand and siltstone rock fragments, and metamorphic rock fragments.

The amount of syntaxial quartz cement varies from 1 to 20.7% by volume in undeformed rock samples (Table 1). Samples from Force Mill (FM) and Lacy's Cave (LC) contain amounts from 1 to 11.7%, whereas samples from Bowscar Quarry (BQ), Red Rock Quarry (RR) and Salter Hill (SH) contain 11 20.7% (Fig. 4a d).

Quartz grains generally exhibit a red coating on the surface, which can be divided into two groups of either pigmented hematite dust rims or illite coatings, commonly stained red by hematite (Fig. 5). Well developed illite coatings were observed in aeolian samples from Force Mill (FM) (Fig. 5e and f) and Lacy's Cave (LC). In areas where a beige colour alteration is observed macroscopically, the illite appears locally unstained in thin section petrography (see below). Where a locally continuous layer of hematite or illite is present on the detrital quartz grain surface, syntaxial overgrowth is not present (arrows in Fig. 4c and d). However, at sites where no continuous grain coating by either mineral is present, syntaxial overgrowth forms and may grow over the incomplete grain coating. The correlation of grain coating coverage with quartz cement emphasizes the strong impact of clay mineral coatings in the study area (Fig. 6). Within a dune sandstone from one dune, the grain coating coverage does not vary systematically (samples BQ 1 to 4).

Table 1. Compilation of point-count (n = 300) results for the samples from the study area including the evaluation of clay coat coverage (n = 50) and additional sample information (i.e. the depositional environment, mean grain size and sorting)

	Bowscar Quarry				Force Mill				Lacy's Cave		Red Rock Quarry					Salter Hill
	BQ 1	BQ 2	BQ 3	BQ 4	FM 1	FM 2	FM 3	FM Alt	LC 1	LC 2	RR 1	RR 2	RR 3	RR 4	RR 5	SH 1
Detritus																
Quartz (including undulose and polycrystalline)	68.3	64.7	71.3	60.0	78.7	67.0	65.7	72.1	71.3	76.0	65.0	66.3	73.0	69.3	70.7	63.7
K-feldspar	2.7	6.3	5.0	6.0	4.0	6.0	4.3	3.0	4.3	2.7	4.7	6.0	2.7	4.3	4.7	4.0
Plagioclase	0.0	0.0	0.0	0.3	0.3	0.3	0.0	0.0	0.3	0.0	0.0	0.7	0.0	0.0	0.0	0.3
Clay matrix	0.0	0.0	0.3	0.0	0.3	0.0	0.0	0.0	0.0	0.0	0.0	0.0	0.0	0.0	0.3	0.3
Mica	0.0	0.0	0.0	0.0	0.0	0.0	0.7	0.0	0.3	0.0	0.0	0.3	0.0	0.7	0.3	0.0
Hematite	0.0	0.0	0.0	0.0	0.0	0.7	0.7	0.0	0.3	0.0	0.0	0.0	0.0	0.0	0.3	0.0
Accessory minerals (titanite, tourmaline, zircon)	0.0	0.0	0.0	0.0	0.0	0.0	0.0	1.0	0.0	0.0	0.3	0.0	0.0	0.0	0.0	0.0
Shale rock fragment	0.0	0.3	0.0	0.0	0.3	0.0	0.0	0.0	0.0	0.0	0.0	0.0	0.0	0.0	0.0	0.7
Sandstone rock fragment	0.0	1.0	0.3	0.0	0.0	0.3	0.0	0.3	0.3	0.3	0.3	0.0	1.0	1.0	0.3	0.3
Volcanic rock fragment	0.3	0.3	0.3	2.0	1.0	1.3	1.0	0.7	1.3	1.0	1.7	1.0	0.7	1.0	0.7	2.0
Plutonic rock fragment	0.0	0.0	0.0	0.3	0.0	0.7	0.7	0.0	0.3	0.0	0.0	0.0	0.3	0.3	0.7	0.0
Metamorphic rock fragment	0.0	0.0	0.0	0.0	0.0	0.7	0.0	0.3	0.0	0.0	0.3	0.0	0.0	0.0	0.0	0.3
Authigenic phases																
Quartz cement	20.7	11.0	11.3	18.0	1.0	11.7	7.0	2.3	5.0	7.3	13.3	14.7	13.7	12.3	5.7	16.5
K-feldspar cement	0.3	0.0	0.0	0.0	0.0	0.3	0.7	0.0	0.0	1.0	0.0	0.0	0.7	0.3	0.0	0.3
Illite pore lining	0.0	1.3	0.3	0.3	1.3	1.3	1.7	4.7	2.3	2.0	2.0	0.0	0.3	0.0	0.7	1.7
Illite pore filling	0.0	0.3	0.0	0.0	1.0	0.0	0.0	3.3	0.3	0.7	0.0	2.0	0.0	0.7	0.0	0.7
Illite replaces K-feldspar	1.0	1.7	0.0	1.7	0.7	2.7	2.0	1.0	2.3	2.7	4.3	4.3	1.7	2.3	3.3	2.3
Kaolinite replaces K-feldspar	1.3	1.3	1.3	0.7	0.3	0.0	0.3	0.7	0.3	0.0	1.3	1.0	1.0	0.7	0.7	1.3
Calcite	0.0	0.0	0.0	0.0	0.0	0.0	0.0	0.3	0.0	0.0	0.0	0.0	0.0	0.0	0.0	0.0
Siderite	0.0	0.0	0.0	0.0	0.0	0.0	0.0	0.3	0.0	0.0	0.0	0.0	0.0	0.0	0.0	0.0
Anhydrite	0.0	0.0	0.0	0.0	0.0	0.0	0.0	0.3	0.0	0.0	0.0	0.0	0.0	0.0	0.3	0.0
Iron oxide pore lining	0.0	0.7	0.3	0.3	0.3	2.0	1.7	0.0	0.7	0.3	0.7	0.0	0.7	0.0	1.0	0.0
Iron oxide pore filling	0.0	1.0	0.0	1.0	0.3	0.0	0.0	0.3	0.0	0.0	1.0	0.3	0.0	0.0	1.0	0.3
Calcite replaces K-feldspar	0.0	0.0	0.0	0.0	0.0	0.0	0.0	0.3	0.0	0.0	0.0	0.0	0.0	0.0	0.0	0.0
Porosity																
Intergranular porosity	5.0	8.0	8.7	9.3	9.3	4.7	13.7	8.6	9.7	5.0	3.7	1.7	4.0	7.0	8.0	4.6
Secondary porosity	0.3	2.0	0.7	0.0	1.0	0.0	0.7	0.3	0.7	0.7	1.7	1.7	0.3	0.0	1.3	0.7
Grain coating coverage																
Grain coating coverage (%)	13.6	25.5	13.9	21.2	95.3	37.1	61.7	83.9	70.1	74.5	31.2	20.3	15.2	19.8	38.2	19.1
Additional sample information																
Depositional environment	Dune	Dune	Dune	Dune	Dune	Dune	Dune	Dune	Dune	Dune	Dune	Dune	Dune	Dune	Dune	Dune
Mean grain size (mm)	0.47	0.36	0.41	0.15	0.34	0.18	0.19	0.17	0.35	0.38	0.29	0.32	0.19	0.20	0.18	0.45
Sorting	ms	mws	ms	ms	mws	ms	ms	ms	mws	ms	mws	mws	ms	ms	ms	mws

BQ, Bowscar Quarry; FM, Force Mill; LC, Lacy's Cave; RR, Red Rock Quarry; SH, Salter Hill; ms, moderately sorted; mws, moderately well sorted.
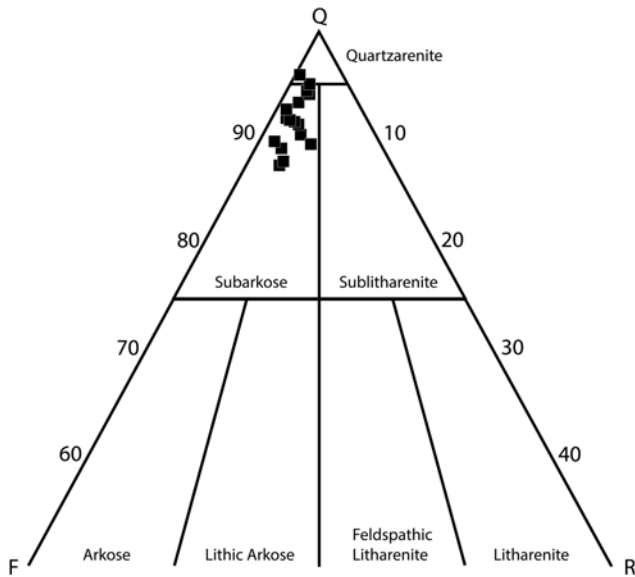
Fig. 2. Ternary quartz feldspar rock fragments (QFR) diagram showing the sample composition from the Vale of Eden.

Carbonate and anhydrite cements in aeolian samples are present in only small quantities around 0.3%. Carbonate cements include calcite and siderite and appear partly dissolved. Dolomite was additionally identified during QEMSCAN® analyses. Dissolved carbonate cements are evident from rhombic pores (dolomoulds) enclosed within quartz overgrowth cements in some aeolian dune samples (Fig. 3a). Rarely, the outcrop samples feature small amounts (0.3%) of anhydrite, present as a grain framework stabilizing and pore filling cement.

QEMSCAN® results

QEMSCAN® analyses can highlight the distribution of mineral phases within the samples. The grain coating characteristics and colour alterations surrounding deformation bands were evaluated using QEMSCAN® analyses.

The quartz content in sample BQ 2 Q (pink, Fig. 7b) is 87.1%. The content of K feldspar (blue green) in the sample from Bowscar Quarry is 6.5%, with some grains partly dissolved (Fig. 4a, b and bottom of Fig. 7b) and some grains kaolinitized or illitized. In the presented sample, the bulk illite content is 3.5% (light green). Kaolinite is sparse at 1.3% (red) whereas chlorite, commonly associated with illite and rock fragments, occurs at 0.7% (green). Considering grain coatings, the fine sand sized grains of the samples from Bowscar Quarry are characterized by a relative enrichment in illite as compared with the coarser grained sand fraction. The fine grained sand fractions of sample BQ 2 Q (lines 3 and 5, Fig. 7a and b) contain $6.1 \pm 0.1\%$ illite (green, Fig. 7b) whereas the coarser intervals (lines 1, 2, 4 and 6, Fig. 7a and b) contain $2.2 \pm 0.7\%$. Additional transmitted light petro graphic analysis highlights the nature of illite in the fine sand fraction as a grain rimming phase and not a pore filling phase (Fig. 7c f).

Oxide phases detected during QEMSCAN® analyses are mainly hematite and rutile grains, which are part of the detrital inventory of the sediment.
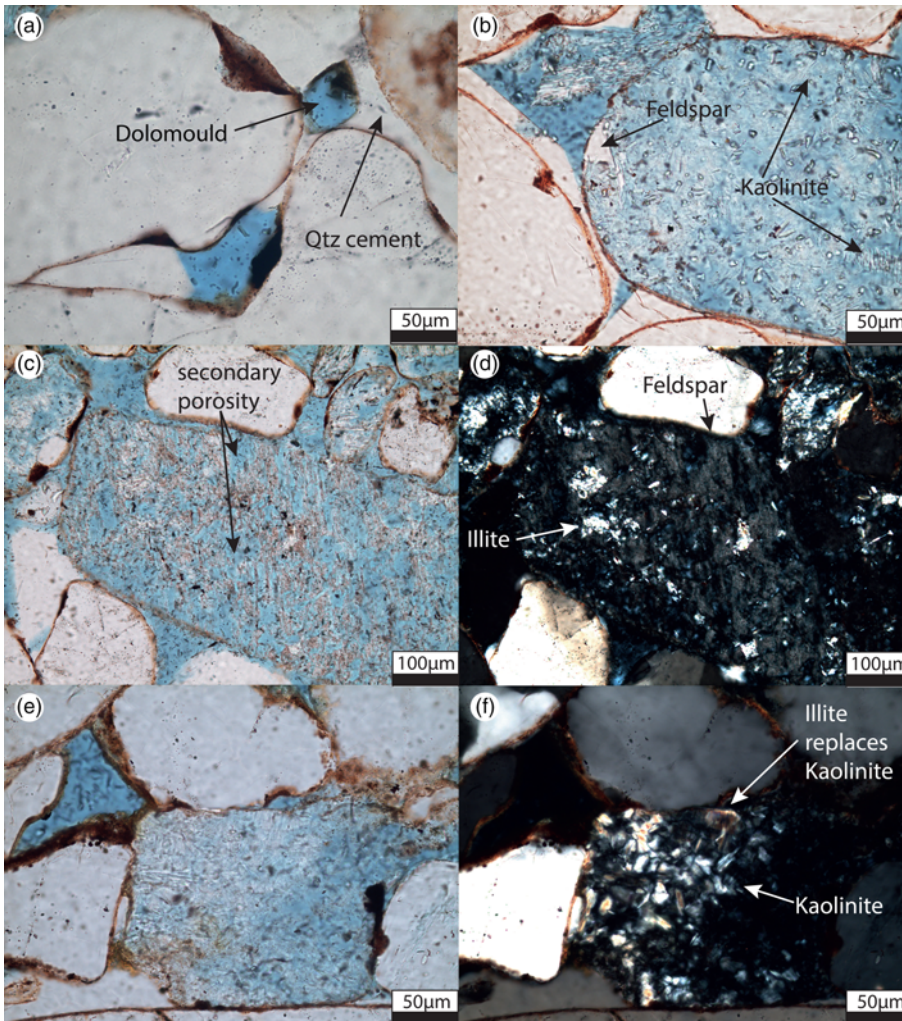

Fig. 3. Prominent authigenic alterations in aeolian samples. (**a**) Dolomould enclosed within syntaxial quartz cements in sample BQ 2. (**b**) Kaolinite replaces feldspar grain while the original grain boundary, marked by pigmented hematite rim, is still preserved in sample BQ 2. (**c, d**) Illite replaces feldspar grain; additionally secondary porosity is generated during the dissolution in sample RR 1. (**e, f**) Kaolinite replaced a detrital grain and is subsequently replaced by illite, still preserving the booklet texture in sample BQ 2. The original grain outline is still preserved, indicating that pervasive grain dissolution and replacive kaolinite formation occurred after significant compaction.
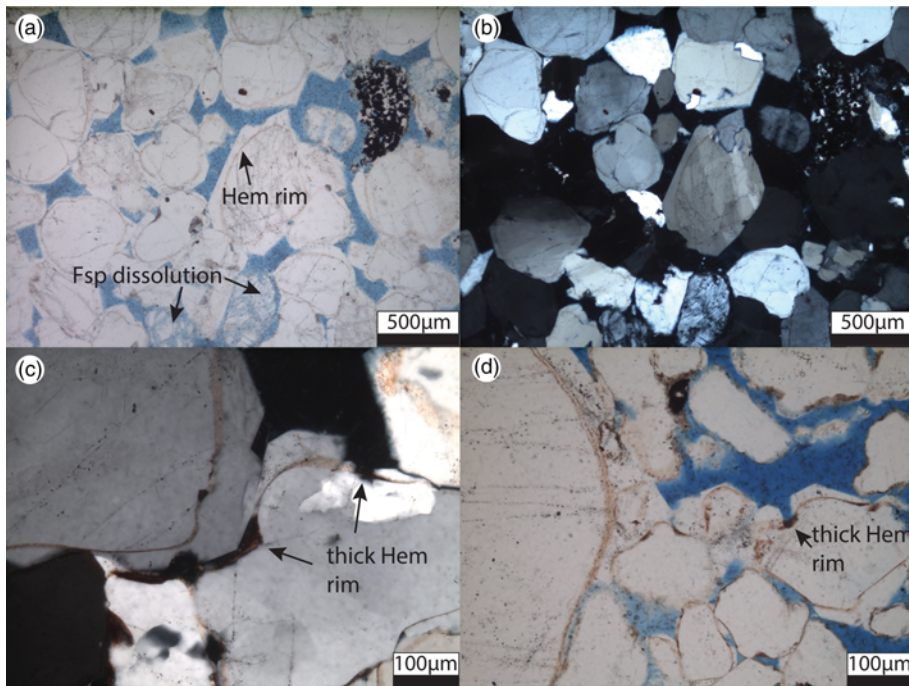
Fig. 4. Aeolian dune samples from Bowscar Quarry. (**a**, **b**) Pigmented hematite dust rims outlining the original grain surface without illite coating the grain surface (BQ 1). (**c**, **d**) Thicker iron oxide and hydroxide linings and occasionally illite inhibit quartz cementation (BQ 1). The thicker continuous iron oxides and hydroxides are accumulated in surface roughnesses and indentations. Hem, hematite; Fsp, K-feldspar.

Bleaching phenomena around deformation bands and faults.

The orientation of deformation bands is illustrated in Figure 8 for the localities at Lacy's Cave (Fig. 8a) and Force Mill (Fig. 8b). Two normal fault planes are exposed in Lacy's Cave and their strike matches the orientation of precursor deformation bands (Fig. 8a, red great circles). At Lacy's Cave and Force Mill, four distinct sets can be distinguished. Conjugate sets of NNW–SSE, NE–SW, and minor west–east and NNE–SSW strikes are present in the exposures. Some deformation bands are characterized by a colour alteration of the red host rock.

Colour alteration was observed around normal faults and deformation bands (also called granulation seams in previous reports from this region) in and around Lacy's Cave and the opposite bank of the River Eden at Force Mill (Fig. 9). The host rock is red some millimetres to centimetres away from a single deformation band or a cluster of deformation bands. In contrast, the host rock surrounding the deformation band or a cluster occasionally appears greyish white (Fig. 9a and b) or beige (Fig. 9c and d). Deformation bands of all strike orientations appear as thin white seams with a surrounding greyish white halo. The beige colour alteration was predominantly observed around deformation bands striking NE–SW. Microscopically, two types of deformation bands can be distinguished in samples from Force Mill. One generation exhibits extensive quartz cementation of cataclastic quartz grains (sample FM 3, Fig. 10a–c),

whereas the other exhibits no overgrowth cementation on the cataclastic grains (sample FM Alt and FM Alt Q, Fig. 11a–d; Table 2). Both have been evaluated microscopically and in the case of sample FM Alt Q, QEMSCAN® analysis aided the evaluation.

The first generation of deformation bands, striking NNW–SSE (260°/58°), is characterized by a greyish white alteration (Fig. 9a and b). Here, the pigmented hematite dust rims are present but overgrown by a later quartz cement phase (Fig. 10a–c). The pigmented hematite dust rims have not been bleached in these deformation bands and the macroscopic colour of the zone around the deformation band is greyish white (Fig. 9a and b). This colour is due to pervasive quartz cementation on freshly broken grains.

The second generation of deformation bands, striking NE–SW (320°/60°), is macroscopically characterized by a beige zone surrounding the deformation band (Fig. 9c and d). Microscopically, both the absence of iron minerals on grain surfaces and colourless clay minerals in the vicinity of the deformation band (Fig. 11a–d) are observed. Some larger hematite grains are still present in the sample (Fig. 12b). Illite is present in the bleached intervals as a pore filling and grain coating phase (Figs 11a, b and 12). Pigmented hematite dust rims occasionally remain at grain contacts. In the undisturbed host rock, the illite coatings are visibly stained red by hematite (Fig. 11e and f). The cataclastic quartz grains are not affected by quartz cementation, and the deformation bands still appear porous (Fig. 11).
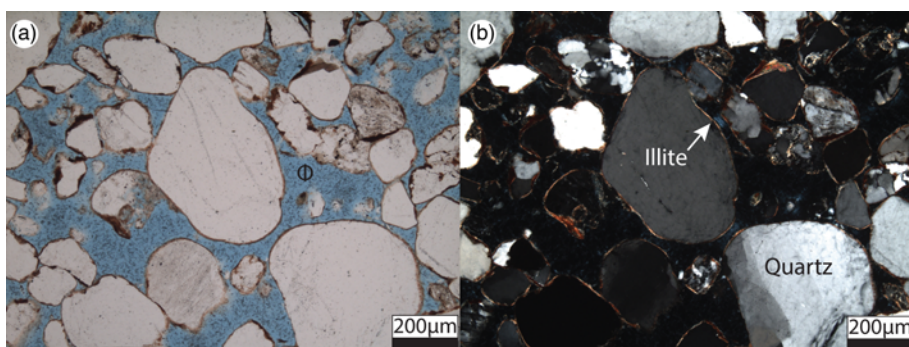

Fig. 5. Micrographs from Force Mill. (**a**, **b**) Intact stained tangential illite coatings are present and inhibit quartz overgrowth cementation in sample FM 1 from Force Mill. φ, blue-dyed pore space.
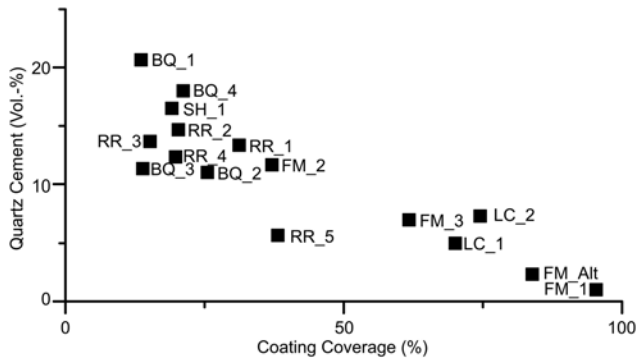
Fig. 6. Correlation between point-counted quartz cement values and observed average grain coat coverage. The decrease in quartz cement correlates well with the grain coat coverage.
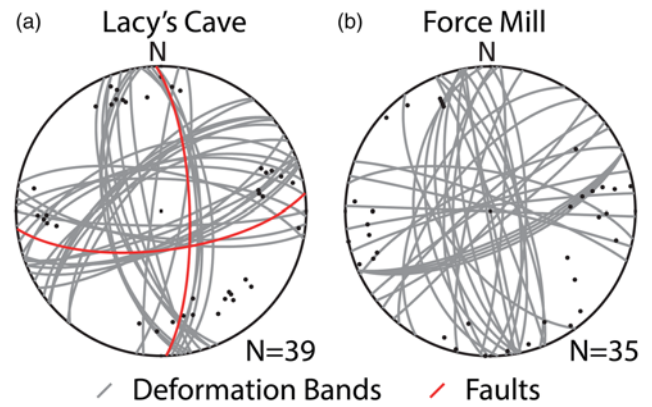

Fig. 8. Compilation of the orientation of deformation bands. (**a**) The measurements from Lacy's Cave feature three distinct orientations (NNW SSE, west east and (E)NE (W)SW) and another minor set (NNE SSW). Two fault planes (red) are exposed and their strike approximately matches the deformation band orientation. (**b**) The deformation band orientation at Force Mill appears more scattered than the nearby Lacy's Cave measurements, but the main orientations are still visible.

Mineralogically, the clay mineral coatings in both the bleached and red parts of the lithology are identified as illite by QEMSCAN® analyses. Microscopically, the red colour is created by small hematite pigments on the mineral surfaces. The QEMSCAN® analyses also highlight a relative increase in illite and kaolinite abundance in the beige alteration haloes as compared with the red sandstones (Fig. 12). The illite abundance is especially increased in the attrition material inside the deformation band (bottom Fig. 12b). In the unbleached part of the formation, the deformation band is mainly characterized by broken K feldspar grains (blue green grains at the bottom in Fig. 12a). Additionally, a difference in grain sizes can be observed. The unbleached interval features a slightly larger average grain size of 0.20 mm compared with 0.18 mm in the bleached interval. Additionally, the sorting after Folk & Ward (1957) in the unbleached part is slightly poorer at 0.72 as compared

with 0.74 in the bleached part, although still being moderately sorted.

Discussion

Petrography and QEMSCAN®

The correlation of standard petrographic point counting analysis and QEMSCAN® analyses is possible to a limited extent. The application of QEMSCAN® analyses in a petrological workflow of sedimentary rocks has been previously established (e.g. Armitage
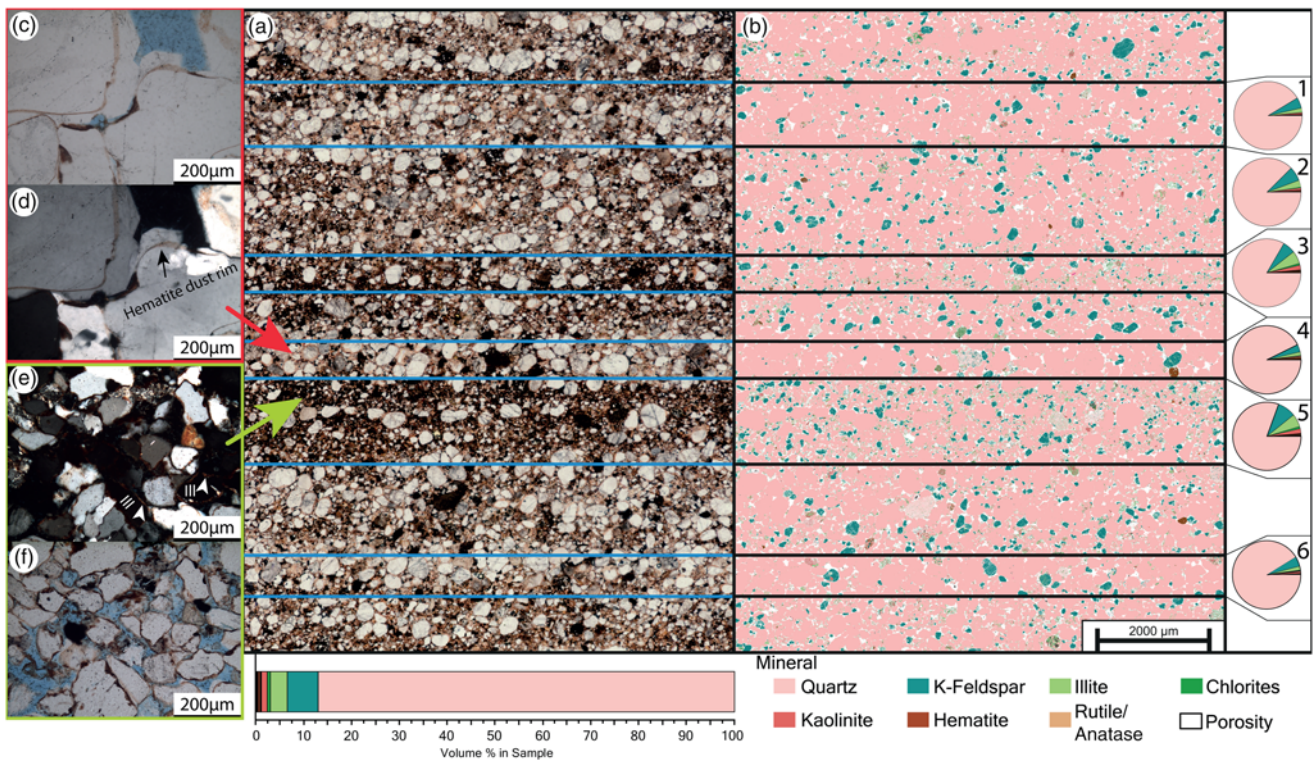

Fig. 7. Comparison of thick-section (100 μm) and QEMSCAN® images of sample BQ 2 Q. (**a, b**) The QEMSCAN® analysis indicates the relative enrichment of illite in the finer grained laminae of the dune sandstone sample from Bowscar Quarry. The delineation of the textures of illite as a pore filling or grain coating phase was made on thin-section images rather than on QEMSCAN® analyses. (**c, d**) Photomicrograph of pigmented hematite dust rims in well-cemented, coarser grained fraction of the sample. (**e, f**) Photomicrograph of the better clay mineral coated, finer grained fraction of the pinstripe-laminated sandstone. This part of the sample contains less quartz overgrowth cement.
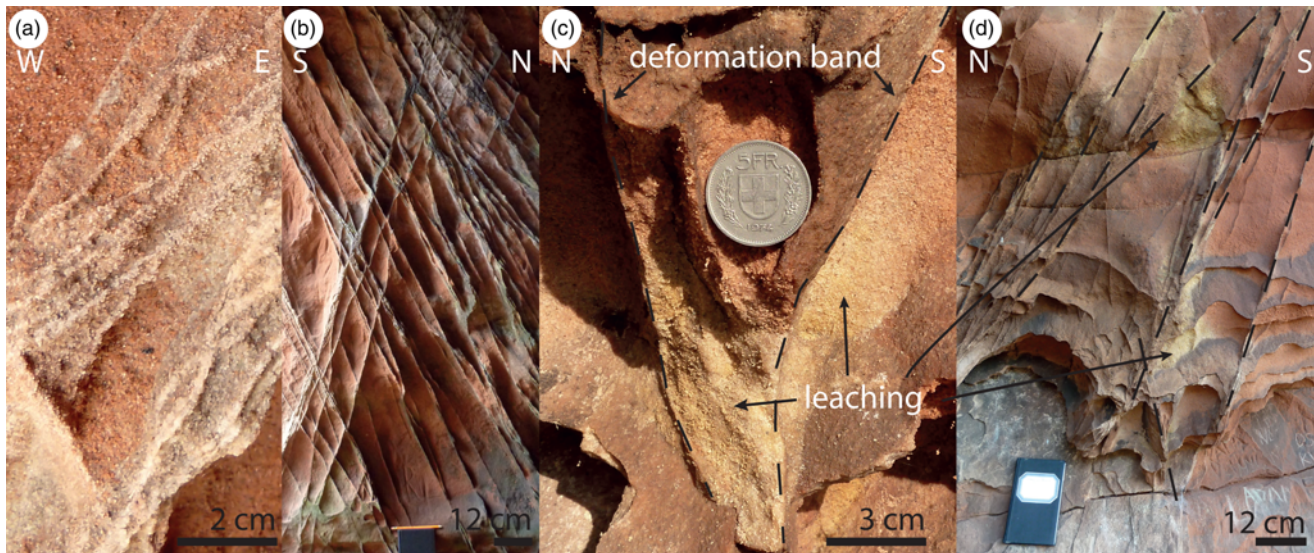
Fig. 9. Deformation band clusters at Lacy's Cave. (**a**, **b**) Greyish-white alteration surrounding a deformation band cluster. The host rock in both cases is still red. (**c**, **d**) Macroscopic image of beige alteration around deformation bands at Lacy's Cave. The alteration is confined to deformation bands.

et al. 2013). However, multiphase grains (i.e. rock fragments) cannot be easily identified as one grain by QEMSCAN® analyses. The detection of multi mineralic rock fragments, which can act as cation donors during diagenesis and bear information on the source area, is not as easy. This also affects the detection of other multi mineralic grains including replacive phases of clay minerals or carbonate or sulphate cements within partly dissolved grains. However, such observations are relevant for interpreting the paragenetic sequence and provenance of the sedimentary rocks. The detrital components (i.e. rock fragments) are also essential in sandstone rock classifications after McBride (1963) or Folk (1980). Additionally, mono and polycrystalline or undulose grains cannot be differentiated by QEMSCAN® analyses although they have an impact on syntaxial quartz cementation (Waugh 1970*a*; Lander *et al.* 2008). Polymorphs of mineral associations cannot be differentiated (Pirrie *et al.* 2004). Similarly, the detection of mineral phases does not differentiate between detrital and authigenic phases of the same mineral type. In contrast, such an analysis is easily performed in the case of quartz with a standard, transmitted light microscope or conventional or SEM based cathodoluminescence (CL) analysis. However, the total number of analysed spots during QEMSCAN® analysis of the presented sample is by far superior to that for standard petrographic point count analyses. Here, 18 932 350 measurements were performed on sample BQ 2 Q (excluding porosity), as compared with 300 point count steps. Additionally, results of QEMSCAN® analyses allow the delineation of mineral associations. Here, the association of a certain mineral phase with another can be quantified. If, however, the correct identification of a mineral phase, because of its limited size, is hindered owing to effects of the excitation volume, these associations are incorrect. Correlations of detected mineral species to grain size, grain shape and porosity (including pore size distribution) are readily available from QEMSCAN® data. The evaluation of certain parts of the sample could highlight the presence of certain mineral species in regard to grain size and porosity. In this study the presence of quartz overgrowth would result in an overestimation of grain size as detected by QEMSCAN® in regard to actual detrital grain sizes.

In the evaluation of clay coating coverage, the current technology is not able to automatically and sufficiently detect grain coating illite in the polished thin section sample. Occasionally, the coating cannot be detected owing to an interference of the grain coating

phase and the substrate grain in EDX analyses. This is due to the small size of particles and the relative size of the excitation volume during EDX analyses (e.g. El Gomati *et al.* 2011). In our study, it is valid for illite grain coatings and pigmented hematite rims. Because transmitted light analyses are used during point counting, hematite on grain surfaces could be detected although the pigments are enclosed in quartz cement and are not present at the thin section surface. Analysis with a method based on an SEM platform performed on polished thin sections will result in true 2D measurements and might, in the case of pigmented hematite contents, deliver more accurate results as opposed to transmitted light analyses. A larger step size during QEMSCAN® analyses to cover a complete thin section sample reduces the maximum file size, but might also be responsible for a possible underestimation of hematite pigments.

Other minerals with low concentrations are visualized by the QEMSCAN® analyses only (e.g. chlorite). Whereas chlorite was not detected by point counting, QEMSCAN® recorded 123 060 occurrences out of 18 932 350 analysed spots in total (0.65%). This is also valid for the quantification of rare heavy mineral species.

The standard petrographic analyses are favoured in the presented case. This also includes the assessment of secondary porosity restricted to certain mineral phases.

The far larger number of analysed points during QEMSCAN® analysis, however, is a better basis for a rigorous statistical approach in analysing mineral occurrence. The automated acquisition of data and large database available for association analyses as well as many automated analyses (grain size, visible porosity, etc.) are benefits of the QEMSCAN® approach.

Petrography

Grain coatings.

Grain coating phases exert a major control on quartz cementation during burial diagenesis (Ajdukiewicz *et al.* 2010; Taylor *et al.* 2010; Ajdukiewicz & Larese 2012). Their presence and extent is reported to be controlled by depositional and climatic processes (Salem *et al.* 2000; Esch *et al.* 2008; Ajdukiewicz *et al.* 2010).

Climatic changes as reported for aeolian settings (Esch *et al.* 2008) might also affect the presence and extent of clay mineral coatings in the Penrith Sandstone Formation. Mader & Yardley (1985) postulated a shift to more humid or semi arid conditions
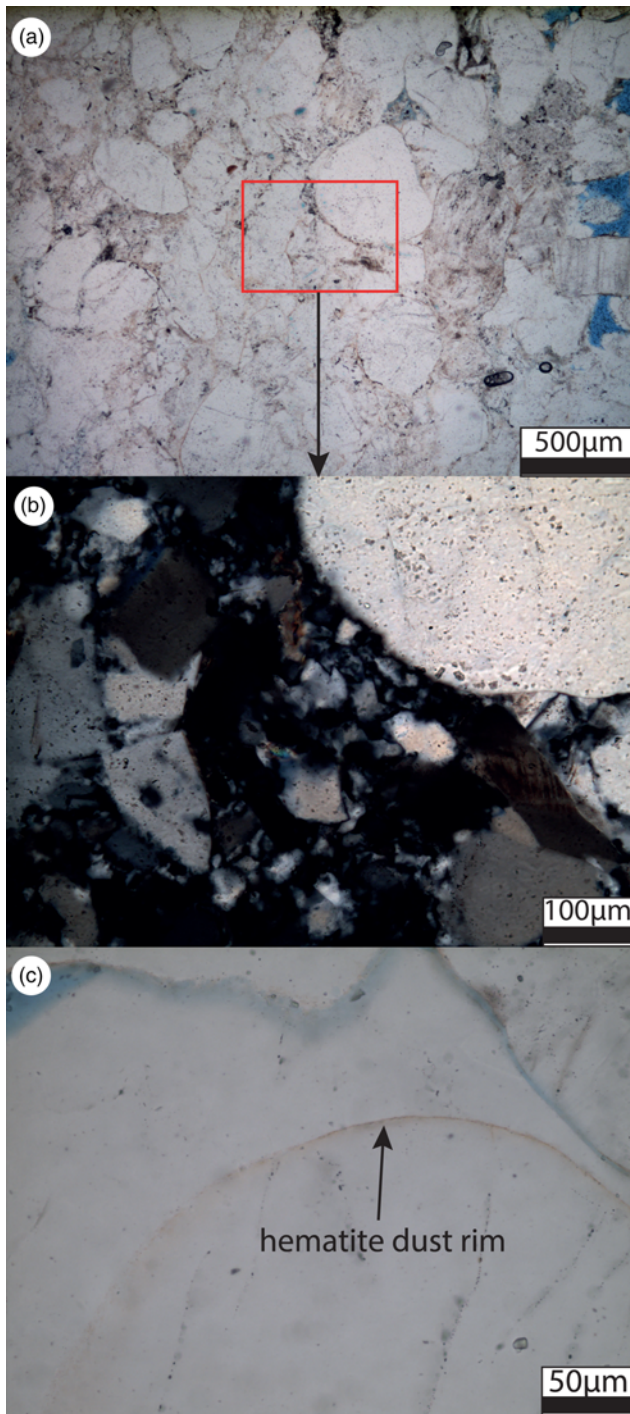
Fig. 10. Deformation band micrographs from Force Mill. (**a**) Quartz-cemented deformation band with no retained porosity in sample FM 3. The undisturbed host rock on the right features pores. (**b**) Magnification of quartz-cemented cataclastic band (red box in (**a**)) showing angular quartz fragments owing to cataclasis, which have been quartz cemented (FM 3). (**c**) Directly surrounding the cataclastic band, quartz cement preserves pigmented hematite dust rims on detrital grains (FM 3).

during the late Permian in this basin. This shift is marked by an increase in the periodicity of ephemeral fluvial intercalations in the Penrith Sandstone Formation towards the Eden Shales Formation (Mader & Yardley 1985). This model of climatic evolution towards less arid conditions would support the increase in grain coating illite present in the formation (see Table 1). Waugh (1970b) reported a less silicified sandstone in association with fluvial deposits in the study area. Another factor affecting the varying amounts of grain coating coverage of illite could be the migration activity of a dune.

Ajdukiewicz *et al.* (2010) proposed an abrasion of coating materials during dune migration, where only smaller grains are able to retain their coating (Wilson 1992). Pigmented hematite dust rims and minor amounts of clay minerals can be preserved during transport owing to surface roughness (Wilson 1992; Fischer *et al.* 2013). This could explain the observed differences in samples from Red Rock and Bowscar Quarry (Fig. 7), where finer grains exhibit larger grain coating coverages. Additionally, the capillary retention capacity of finer grained layers could explain such differences if the clay minerals are infiltrated (Smith *et al.* 1930). Here, the retained water allows the accumulation of infiltrated clay minerals in an early diagenetic environment, whereas the fluids percolate more easily through the matrix created by coarser grains.

Paragenetic sequence.

The petrographic observations in correlation with the literature result in the following paragenetic sequence (Fig. 13).

Early diagenesis.

The earliest diagenetic alteration was the formation of hematite and detrital clay mineral rims as observed for other red beds and aeolianites (van Houten 1973; Ajdukiewicz *et al.* 2010). The clay mineral rims have a considerable impact on the inhibition of syntaxial quartz cement growth in the study area (Fig. 6).

Where carbonate cements, here calcite, dolomite and siderite, are still present, they appear to be pore filling and grain framework stabilizing, and are interpreted to be of an early diagenetic origin. Because of the arid depositional environment during the Cisuralian and limited textural evidence, the carbonate formation is thought to occur during early diagenesis and contemporaneously with deposition (Morad *et al.* 2000) (Fig. 13). Small rhombic pores inside quartz cements were previously linked to early dolomite cementation (see fig. 8 of Waugh 1970b; Turner *et al.* 1995). An early anhydrite phase is evident from textural relations appearing as grain framework stabilizing pore fillings.

Feldspar dissolution and kaolinite authigenesis is interpreted to occur in an early and a late stage of diagenesis (Lanson *et al.* 2002). The early phase is marked by later burial diagenetic alteration to illite (type II).

Burial diagenesis.

Quartz overgrowth formation during burial occurred in both the host rock and previously faulted rocks. Turner *et al.* (1995) linked two discrete growth patterns in CL analyses in samples from the Vale of Eden to two discrete quartz cementation phases (their fig. 3a c). However, these two different growth patterns have also been reported to form during noneuhedral *c* axis growth and subsequent pyramidal face growth during continuous overgrowth (Lander *et al.* 2008, figs 9 and 18). The models of Lander *et al.* (2008) assume a continuous quartz cement growth and are able to reproduce natural datasets (Harwood *et al.* 2013).

Quartz overgrowth is locally inhibited by the presence of extensive grain coating coverages. Variations in quartz cementation can be explained by the localized occurrence of illitic coatings (see Fig. 6), which are described to limit syntaxial overgrowth cementation (Storvoll *et al.* 2002). Earlier work by Waugh (1970*a*, *b*) described the presence of illite and hematite on grain surfaces but did not consider a quantitative correlation (Fig. 6). The hematite stain (as pigmented hematite dust rims or intermixed with illite grain coatings) is present at all exposures but the occurrence of illite and its grain coating coverage varies strongly within the sampled parts of the Penrith Sandstone Formation.

The fluid chemistry during quartz cementation has been rather well constrained by fluid inclusion analyses of samples from the
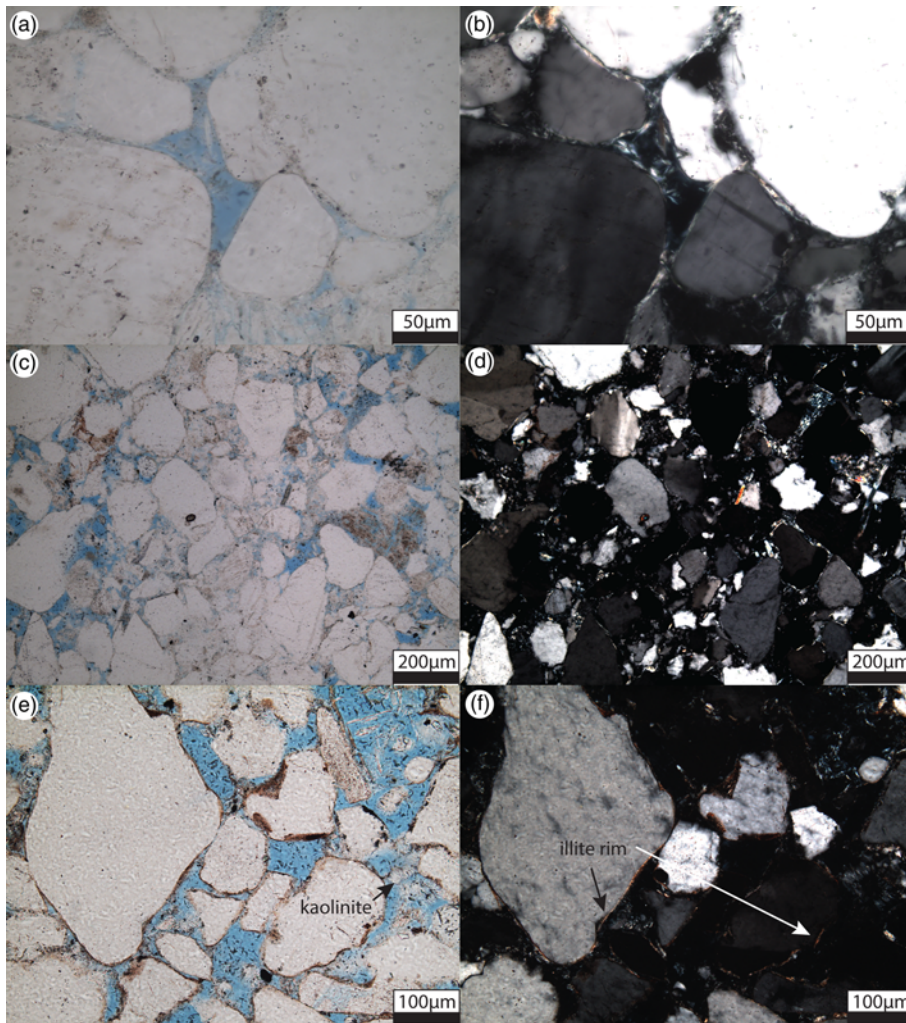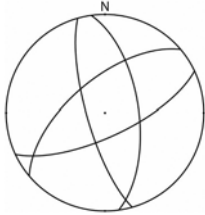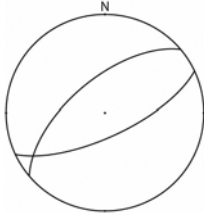
Fig. 11. Cataclastic deformation band from Force Mill (all images from sample FM Alt) (**a**, **b**) Illite coatings from a bleached part of the lithology close to a deformation band at Force Mill. The illite coatings can clearly be distinguished by the interference colours. (**c**, **d**) Overview of the cataclastic deformation band. Some porosity is retained within the band. Additionally, the pigmented hematite dust rims are absent. (**e**, **f**) Approximately 2 mm away from the deformation band cluster, the illite rims still appear with a reddish-brown stain by hematite. Pore-filling kaolinite is present as an alteration product of feldspars and appears unillitized in this case.

Penrith Sandstone Formation by Turner *et al.* (1995) and points towards an alkaline milieu, reaching maximum temperatures of *c.* 120°C. The alteration of precursor clay phases on grain surfaces towards illite and the illitization of feldspars is also interpreted to occur in this higher temperature domain (Worden & Morad 2002)

Table 2. *Schematic comparison of the two main deformation band generations based on macroscopic and microscopic alterations*

Sample	Figures 9a, b and 10a c	Figures 9c, d and 11a d
Colour of halo	Greyish white	Beige
Strike		
Cataclasis	Yes	Yes
Quartz cement	Yes	No
Bleaching	No	Yes
Pigmented hematite dust rim (inside deformation band)	Yes	No
Timing	Before burial diagenesis	After burial diagenesis

Samples from both major strike directions appear grey to white, whereas the beige alteration is confined to the NE SW-striking set.

(Fig. 13). The replacement of parts of the first kaolinite phase by illite is kinetically controlled during burial diagenesis (e.g. Lander & Bonnell 2010). This alteration is additionally controlled by the amounts of K feldspar still present during burial diagenesis, acting as a source for potassium (Ehrenberg & Nadeau 1989). Because all three reactants are available in the samples, the process is not expected to have ceased during burial diagenesis.

Evident from magnetic remanence experiments on samples from the Penrith Sandstone Formation by Turner *et al.* (1995), hematite authigenesis occurred continuously throughout the burial history.

The alteration of rock fragments and pore filling precursor clay minerals to chlorite is expected to be a burial related alteration (Boles & Franks 1979; De Ros *et al.* 1994; Hillier 1994; Remy 1994; Worden & Morad 2002).

Uplift diagenesis.

Remnants of carbonate and sulphate cements in these exposed Rotliegend rocks appear partly dissolved as a result of interaction with meteoric waters. The carbonate and sulphate cements have been reported from the subsurface (Arthurton & Wadge 1981; Turner *et al.* 1995). A second, unillitized phase of kaolinite (type I) is interpreted to have formed during late uplift, owing to exposure related diagenesis and interaction with meteoric waters (Lanson *et al.* 2002) (Fig. 13).

Structural development and bleaching

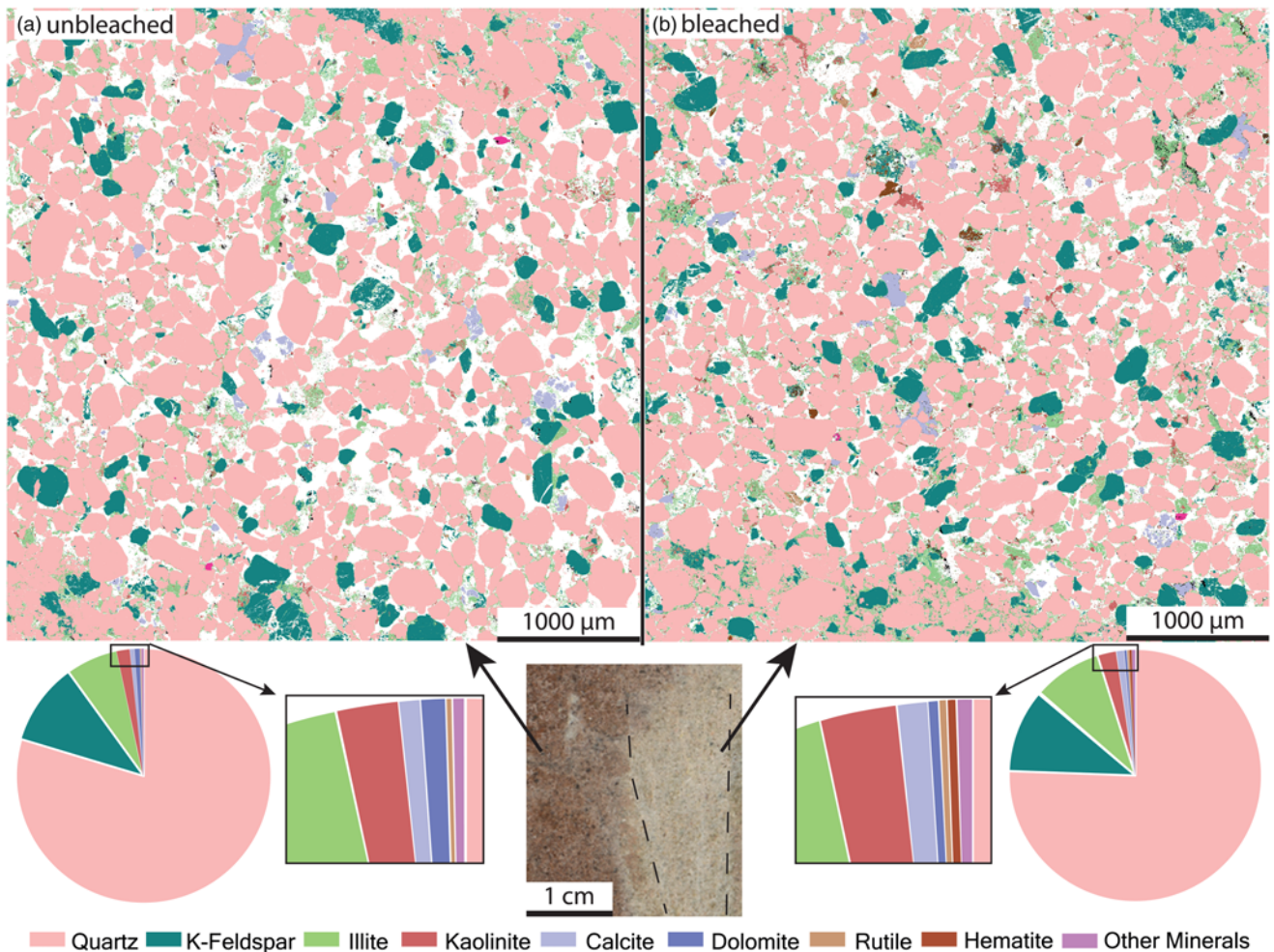The alterations surrounding deformation bands and their structural orientations are compiled in Table 2.

Fig. 12. Comparison of the mineralogical suite of regular (**a**) and bleached (**b**) sandstone around deformation bands at a beige alteration zone in the Penrith Sandstone (centre image) using QEMSCAN® in sample FM Alt. The dashed lines in the specimen photograph outline the multistrand cataclastic band. The bleached interval (**b**) contains relatively more illite (green) and kaolinite (red) than the unbleached rock (**a**). The white area between grains represents porosity filled by an epoxy resin.

Greyish-white alteration.

The observed greyish white colour alteration of a NNW SSE striking deformation band cluster at Force Mill and Lacy's Cave is interpreted to be mainly controlled by a pore filling quartz cement phase that preserves pigmented hematite dust rims (see Fig. 10a c). This phase of deformation band formation is thus not affected by bleaching processes. The deformation bands thus predate syntaxial quartz cementation during burial diagenesis. The structural orientation of a quartz cemented, unbleached, potentially earlier set of deformation bands approximately matches the strike of the large NW SE Pennine Fault. This colour alteration was also macroscopically observed around deformation bands striking NW SE.

Beige alteration.

The observed beige alteration halo around NE SW striking deformation bands is interpreted to be a product of hematite dissolution and transport, as little to no hematite is present on grain surfaces or intermixed with the illite coatings (Fig. 11a d).

Turner *et al.* (1995) suggested alkaline fluids originating from the Eden Shales Formation to be present during quartz cementation and hematite authigenesis. Their argument is supported by fluid inclusion analyses. However, alkaline fluids tend not to dissolve hematite under oxidizing conditions, which are considered to have been prevailing during quartz cementation (Turner *et al.* 1995;

Takeno 2005). As presented by Parry *et al.* (2004), reducing organic fluids and hydrocarbons are able to cause sandstone bleaching of red beds. More generally, the dissolution of iron bearing minerals is favoured by acidic conditions and reducing fluids (Tucker 2001; Takeno 2005).

The different fluid chemistries during diagenesis need to accommodate (1) alkaline, oxidizing and saline conditions during quartz cementation and hematite authigenesis and (2) acidic and reducing conditions during bleaching.

A source for the latter fluid type could be the Upper Carboniferous coal seams (see Platt 1993). The Appleby Group in the northern part of the Vale of Eden half graben unconformably overlies Upper Carboniferous strata containing the Coal Measures and Millstone Grit including coal seams (see Arthurton & Wadge 1981; Hughes 2003). However, no further evidence was found to constrain the fluid composition or source. At the time of the second deformation band formation, temperatures in the underlying Upper Carboniferous might also be too low for hydrocarbon expulsion (see Fig. 13), which starts at temperatures of *c.* 100°C (see Platt 1993).

The absence of quartz overgrowth on cataclastic grains within the associated deformation band allows another constraint. The migration of the bleaching fluids through the Penrith Sandstone and the formation of the deformation band has to postdate extensive quartz cementation. Broken grains still appear uncemented, although they commonly present favourable sites for quartz cementation (Fisher *et al.* 2000). Some examples in this study and
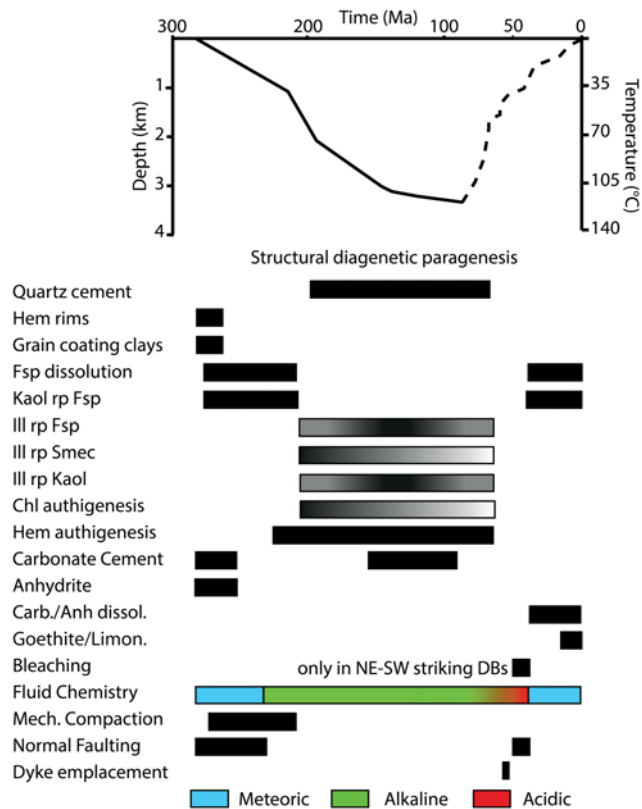
Fig. 13. Reconstructed burial curve from Turner *et al.* (1995), and the presented paragenetic sequence. Replacements are indicated by the term rp, with the replacing phase being named first. The potential illitization of smectitic precursor grain coats is interpreted to stop once the precursor smectite is consumed, as indicated by the shaded box. Transformation to chlorite is also expected to cease once the reactants are consumed. Hem, hematite; Fsp, feldspar; Kaol, kaolinite; Ill, illite; Smec, smectite; Chl, chlorite; Carb, carbonate; Anh, anhydrite; Limon., limonite; DB, deformation band.

from the study by Fowles & Burley (1994) exhibit no syntaxial overgrowth cementation inside cataclastic deformation bands, which suggests that they formed after the pervasively quartz cemented deformation bands. In this study the bleaching was examined on a deformation band sample striking NE SW. Normal faults of a similar strike displacing the Armathwaite dyke point towards a formation postdating the emplacement during the Tertiary (Fowles & Burley 1994). This would require a phase of extensive tectonics featuring normal faulting briefly interrupting the uplift of the area since the Tertiary (Fig. 13).

Considering the timing of fluid flow, Fowles & Burley (1994) assumed the deformation bands and fault clusters to be transmissive only during and shortly after faulting. Their analyses showed a zone of increased permeability around deformation bands. The deform ation bands enhanced fluid flow in a limited zone parallel to their extent (Fowles & Burley 1994). The bleaching in the closely fault associated host rock should be contemporaneous with or slightly postdating the formation of the bands. The host rock at outcrop appears friable and largely uncemented. Bleaching during exposure would probably result in a more homogeneous bleaching pattern in the formation. However, the absence of both quartz overgrowth cement and clay mineral coatings on freshly broken quartz surfaces suggests formation at temperatures below *c.* 70°C and postdating pervasive quartz cementation.

The limited lateral extent of the beige alteration could be explained by pervasive carbonate and sulphate cementation of the strata in the subsurface, which is documented in shallow boreholes (Arthurton & Wadge 1981; Turner *et al.* 1995).

Conclusions

(1) QEMSCAN® can deliver valuable information on low concentration detrital and authigenic phases in sandstones. A combination of transmitted light microscopy and/or CL with QEMSCAN® could result in an improvement of quantitative and qualitative analysis during the assessment of diagenetic alterations in sandstones. To date, however, petrographic analysis is indispensable for grain coat analyses and reservoir quality analysis and modelling.

(2) This study shows that grain coating coverages in the studied samples correlate well with observed quartz cement volumes and highlight the importance of clay coatings for sandstone cementation. They are a key to decipher the structural and diagenetic development as they retained hematite within their fabric and inhibited quartz cement growth. Only where the illite hematite mixture is in contact with the pore fluid can it record the localized bleaching postdating pervasive quartz cementation.

(3) At least two phases of normal faulting and associated deformation band formation occurred and can be dated relative to burial diagenetic alterations. The first, unbleached, NNW SSE and NE SW striking orientation predates or is contemporaneous with early burial diagenesis. The second phase resulted in a bleached (beige), NE SW orientation postdating burial diagenetic alterations and includes evidence of hematite leaching during fault focused fluid migration.

(4) The linked structural and diagenetic evolution is important for hydrocarbon migration and entrapment. The suitability of the studied exposures as direct analogues for subsurface reservoirs is reduced as uncemented cataclastic deformation bands are not expected in reservoirs at depth with temperatures above *c.* 70°C. Their character as palaeo fluid pathways, however, is still indicated by bleaching around deformation bands.

References

Aagaard, P., Jahren, J.S., Harstad, A.O., Nilsen, O. & Ramm, M. 2000. Formation of grain-coating chlorite in sandstones. Laboratory synthesized vs. natural occurrences. *Clay Minerals*, **35**, 261 269, https://doi.org/10.1180/000985500546639

Ajdukiewicz, J.M. & Larese, R.E. 2012. How clay grain coats inhibit quartz cement and preserve porosity in deeply buried sandstones: Observations and experiments. *AAPG Bulletin*, **96**, 2091 2119, https://doi.org/10.1306/02211211075

Ajdukiewicz, J.M., Nicholson, P.H. & Esch, W.L. 2010. Prediction of deep reservoir quality using early diagenetic process models in the Jurassic Norphlet Formation, Gulf of Mexico. *AAPG Bulletin*, **94**, 1189 1227, https://doi.org/10.1306/04211009152

Antonellini, M. & Aydin, A. 1994. Effect of faulting on fluid flow in porous sandstones: Petrophysical properties. *AAPG Bulletin*, **78**, 355 377.

Antonellini, M. & Aydin, A. 1995. Effect of faulting on fluid flow in porous sandstones: Geometry and spatial distribution. *AAPG Bulletin*, **79**, 642 671.

Armitage, P.J., Worden, R.H., Faulkner, D.R., Aplin, A.C., Butcher, A.R. & Espie, A.A. 2013. Mercia Mudstone Formation caprock to carbon capture and storage sites: petrology and petrophysical characteristics. *Journal of the Geological Society, London*, **170**, 119 132, https://doi.org/10.1144/jgs2012-049

Arthurton, R.S. & Wadge, A.J. 1981. *Geology of the country around Penrith*. Memoirs of the Geological Survey of Great Britain. HMSO, London.

Boles, J.R. & Franks, S.G. 1979. Clay diagenesis in Wilcox sandstones of Southwest Texas; implications of smectite diagenesis on sandstone cementation. *Journal of Sedimentary Petrology*, **49**, 55 70. https://doi.org/10.1306/212F76BC-2B24-11D7-8648000102C1865D

Busch, B., Winkler, R., Osivandi, K., Nover, G., Amann-Hildenbrand, A. & Hilgers, C. 2017. Evolution of small-scale flow barriers in German Rotliegend siliciclastics. *In*: Armitage, P.J., Butcher, A.R., Churchill, J.M., Csoma, A.E., Hollis, C., Lander, R.H., Omma, J.E. & Worden, R.H. (eds) *Reservoir Quality of Clastic and Carbonate Rocks: Analysis, Modelling and Prediction*. Geological Society, London, Special Publications, **435**, https://doi.org/10.1144/sp435.3

De Ros, L.F., Anjos, S.M.C. & Morad, S. 1994. Authigenesis of amphibole and its relationship to the diagenetic evolution of Lower Cretaceous sandstones of the Potiguar rift basin, northeastern Brazil. *Sedimentary Geology*, **88**, 253 266, https://doi.org/10.1016/0037-0738(94)90065-5

Ehrenberg, S.N. & Nadeau, P.H. 1989. Formation of diagenetic illite in sandstones of the Garn Formation, Haltenbanken area, Mid-Norwegian continental shelf. *Clay Minerals*, **24**, 233 253, https://doi.org/10.1306/BDFF8E5C-1718-11D7-8645000102C1865D

Eichhubl, P. & Flodin, E. 2005. Brittle deformation, fluid flow, and diagenesis in sandstones at Valley of Fire State Park, Nevada. *In*: Pederson, J. & Dehler, C. M. (eds) *Interior Western United States*. Geological Society of America Field Guide, **6**, 151 167, https://doi.org/10.1130/2005.fl

Eichhubl, P., Taylor, W.L., Pollard, D.D. & Aydin, A. 2004. Paleo-fluid flow and deformation in the Aztec Sandstone at the Valley of Fire, Nevada Evidence for the coupling of hydrogeologic, diagenetic, and tectonic processes. *Geological Society of America Bulletin*, **116**, 1120 1131, https://doi.org/10.1130/b25446.1

El-Gomati, M.M., Walker, C.G.H. & Zha, X. 2011. Towards quantitative scanning electron microscopy: Applications to nano-scale analysis. *Nuclear Instruments and Methods in Physics Research, Section A*, **645**, 68 73, https://doi.org/10.1016/j.nima.2010.12.133

Esch, W.L., Ajdukiewicz, J.M. & Reynolds, A.C. 2008. Early grain-coat formation in Chaco dune field, New Mexico: insight into formation mechanisms, distribution, and implications for predictive modeling to assist in deep play identification [abstract]. AAPG Annual Convention, 20-23 April, San Antonio, TX, Search and Discovery Article #50135.

Fischer, C., Aurin, P., Darbha, G.K. & Arp, G. 2013. Experimental approaches to the formation of early-diagenetic grain coats on quartz surfaces. *Zeitschrift der Deutschen Gesellschaft für Geowissenschaften*, **164**, 225 236, https://doi.org/10.1127/1860-1804/2013/0030

Fisher, Q.J. & Knipe, R. 2001. Permeability of faults within siliciclastic petroleum reservoirs of the North Sea and Norwegian continental shelf. *Marine and Petroleum Geology*, **18**, 1063 1081.

Fisher, Q.J., Knipe, R.J. & Worden, R.H. 2000. Microstructures of deformed and non-deformed sandstones from the North Sea: implications for the origins of quartz cement in sandstones. *In*: Worden, R.H. & Morad, S. (eds) *Quartz Cementation in Sandstones*. Blackwell Science, Oxford, 129 146, https://doi.org/10.1002/9781444304237.ch10

Folk, R.L. 1980. *Petrology of Sedimentary Rocks*. Hemphill, Austin, TX.

Folk, R.L. & Ward, W. 1957. Brazos River bar: a study in the significance of grain-size parameters. *Journal of Sedimentary Petrology*, **27**, 3 26, https://doi.org/10.1306/74D70646-2B21-11D7-8648000102C1865D

Fossen, H. & Bale, A. 2007. Deformation bands and their influence on fluid flow. *AAPG Bulletin*, **91**, 1685 1700, https://doi.org/10.1306/07300706146

Fossen, H. & Rotevatn, A. 2012. Characterization of deformation bands associated with normal and reverse stress states in the Navajo Sandstone, Utah: Discussion. *AAPG Bulletin*, **96**, 869 876, https://doi.org/10.1306/09221110173

Fossen, H., Schultz, R.A., Shipton, Z.K. & Mair, K. 2007. Deformation bands in sandstone: A review. *Journal of the Geological Society, London*, **164**, 1 15, https://doi.org/10.1144/0016-76492006-036

Fowles, J. & Burley, S.D. 1994. Textural and permeability characteristics of faulted, high porosity sandstones. *Marine and Petroleum Geology*, **11**, 608 623, https://doi.org/10.1016/0264-8172(94)90071-X

Guo, J., McCaffrey, K., Jones, R. & Holdsworth, R. 2009. The spatial heterogeneity of structures in high porosity sandstones: Variations and granularity effects in orientation data. *Journal of Structural Geology*, **31**, 628 636, https://doi.org/10.1016/j.jsg.2008.12.002

Harwood, J., Aplin, A.C., Fialips, C.I., Iliffe, J., Kozdon, R., Ushikubo, T. & Valley, J.W. 2013. Quartz cementation history of sandstone revealed by high-resolution SIMS oxygen isotope analysis. *Journal of Sedimentary Research*, **83**, 522 530, https://doi.org/10.2110/jsr.2013.29

Hillier, S. 1994. Pore-lining chlorites in siliciclastic reservoir sandstones: Electron microprobe, SEM and XRD data, and implications for their origin. *Clay Minerals*, **29**, 665 679.

Hughes, R.A. 2003. *Permian and Triassic rocks of the Appleby district (part of Sheet 30, England and Wales)*. British Geological Survey, Keyworth.

Johansen, T.E.S. & Fossen, H. 2008. Internal geometry of fault damage zones in interbedded siliciclastic sediments. *In*: Wibberley, C.A.J., Kurz, W., Imber, J., Holdsworth, R.E. & Collettini, C. (eds) *The Internal Structure of Fault Zones: Implications for Mechanical and Fluid-Flow Properties*. Geological Society, London, Special Publications, **299**, 35 56, https://doi.org/10.1144/sp299.3

Lander, R.H. & Bonnell, L.M. 2010. A model for fibrous illite nucleation and growth in sandstones. *AAPG Bulletin*, **94**, 1161 1187, https://doi.org/10.1306/04211009121

Lander, R.H., Larese, R.E. & Bonnell, L.M. 2008. Toward more accurate quartz cement models: The importance of euhedral versus noneuhedral growth rates. *AAPG Bulletin*, **92**, 1537 1563, https://doi.org/10.1306/07160808037

Lanson, B., Beaufort, D., Berger, G., Bauer, A., Cassagnabère, A. & Meunier, A. 2002. Authigenic kaolin and illitic minerals during burial diagenesis of sandstones: a review. *Clay Minerals*, **37**, 1 22, https://doi.org/10.1180/0009855023710014

Macchi, L.C. 1981. *Sedimentology of the Penrith Sandstone and brockrams (Permo-Triassic) of Cumbria, north-west England: Volume 1*. PhD thesis, University of Hull.

MacDonald, R., Wilson, L., Thorpe, R.S. & Martin, A. 1988. Emplacement of the Cleveland Dyke: Evidence from geochemistry, mineralogy and physical modelling. *Journal of Petrology*, **29**, 559 583, https://doi.org/10.1093/petrology/29.3.559

Mader, D. & Yardley, M.J. 1985. Migration, modification and merging in aeolian systems and the significance of the depositional mechanisms in Permian and Triassic dune sands of Europe and North America. *Sedimentary Geology*, **43**, 85 218, https://doi.org/10.1016/0037-0738(85)90056-9

McBride, E.F. 1963. A classification of common sandstones. *Journal of Sedimentary Petrology*, **33**, 664 669.

Morad, S., Ketzer, J.M. & De Ros, L.F. 2000. Spatial and temporal distribution of diagenetic alterations in siliciclastic rocks: implications for mass transfer in sedimentary basins. *Sedimentology*, **47**, 95 120, https://doi.org/10.1046/j.1365-3091.2000.00007.x

Nixon, C.W., Sanderson, D.J., Dee, S.J., Bull, J.M., Humphreys, R.J. & Swanson, M.H. 2014. Fault interactions and reactivation within a normal-fault network at Milne Point, Alaska. *AAPG Bulletin*, **98**, 2081 2107, https://doi.org/10.1306/04301413177

Parry, W.T., Chan, M.A. & Beitler, B. 2004. Chemical bleaching indicates episodes of fluid flow in deformation bands in sandstone. *AAPG Bulletin*, **88**, 175 191, https://doi.org/10.1306/09090303034

Paxton, S.T., Szabo, J.O., Ajdukiewicz, J.M. & Klimentidis, R.E. 2002. Construction of an intergranular volume compaction curve for evaluating and predicting compaction and porosity loss in rigid-grain sandstone reservoirs. *AAPG Bulletin*, **86**, 2047 2067, https://doi.org/10.1306/61EEDDFA-173E-11D7-8645000102C1865D

Pirrie, D., Butcher, A.R., Power, M.R., Gottlieb, P. & Miller, G. 2004. Rapid quantitative mineral and phase analysis using automated scanning electron microscopy (QemSCAN); potential applications in forensic geoscience. *In*: Pye, K. & Croft, D.J. (eds) *Forensic Geoscience: Principles, Techniques and Applications*. Geological Society, London, Special Publications, **232**, 123 136, https://doi.org/10.1144/GSL.SP.2004.232.01.12

Platt, J.D. 1993. Controls on clay mineral distribution and chemistry in the early Permian Rotliegend of Germany. *Clay Minerals*, **28**, 393 416, https://doi.org/10.1180/claymin.1993.028.3.05

Remy, R.R. 1994. Porosity reduction and major controls on diagenesis of Cretaceous Paleocene volcaniclastic and arkosic sandstone, Middle Park Basin, Colorado. *Journal of Sedimentary Research*, **A64**, 797 806, https://doi.org/10.1306/D4267EC9-2B26-11D7-8648000102C1865D

Rotevatn, A., Fossen, H., Hesthammer, J., Aas, T.E. & Howell, J.A. 2007. Are relay ramps conduits for fluid flow? Structural analysis of a relay ramp in Arches National Park, Utah. *In*: Lonergan, L., Jolly, R.J.H., Rawnsley, K. & Sanderson, D.J. (eds) *Fractured Reservoirs*. Geological Society, London, Special Publications, **270**, 55 71, https://doi.org/10.1144/gsl.sp.2007.270.01.04

Salem, A.M., Morad, S., Mato, L.F. & Al-Aasm, I.S. 2000. Diagenesis and reservoir-quality evolution of fluvial sandstones during progressive burial and uplift: Evidence from the Upper Jurassic Boipeba Member, Recôncavo Basin, Northeastern Brazil. *AAPG Bulletin*, **84**, 1015 1040, https://doi.org/10.1306/A9673B9E-1738-11D7-8645000102C1865D

Smith, W.O., Foote, P.D. & Busang, P.F. 1930. Capillary retention of liquids in assemblages of homogeneous spheres. *Physical Review*, **36**, 524 530, https://doi.org/10.1103/PhysRev.36.524

Storvoll, V., Bjørlykke, K., Karlsen, D. & Saigal, G. 2002. Porosity preservation in reservoir sandstones due to grain-coating illite: a study of the Jurassic Garn Formation from the Kristin and Lavrans fields, offshore Mid-Norway. *Marine and Petroleum Geology*, **19**, 767 781, https://doi.org/10.1016/S0264-8172(02)00035-1

Takeno, N. 2005. *Atlas of Eh pH diagrams: Intercomparison of thermodynamic databases*. Geological Survey of Japan, Tsukuba.

Taylor, T., Stancliffe, R., Macaulay, C. & Hathon, L. 2004. High temperature quartz cementation and the timing of hydrocarbon accumulation in the Jurassic Norphlet sandstone, offshore Gulf of Mexico, USA. *In*: Cubitt, J.M., England, W.A. & Larter, S. (eds) *Understanding Petroleum Reservoirs: Towards an Integrated Reservoir Engineering and Geochemical Approach*. Geological Society, London, Special Publications, **237**, 257 278, https://doi.org/10.1144/GSL.SP.2004.237.01.15

Taylor, T.R., Giles, M.R. *et al.*et al. 2010. Sandstone diagenesis and reservoir quality prediction: Models, myths, and reality. *AAPG Bulletin*, **94**, 1093 1132, https://doi.org/10.1306/04211009123

Taylor, T.R., Kittridge, M.G., Winefield, P., Bryndzia, L.T. & Bonnell, L.M. 2015. Reservoir quality and rock properties modeling Triassic and Jurassic sandstones, greater Shearwater area, UK Central North Sea. *Marine and Petroleum Geology*, **65**, 1 21, https://doi.org/10.1016/j.marpetgeo.2015.03.020

Tucker, M.E. 2001. *Sedimentary Petrology*, 3rd edn. Blackwell Science, Oxford.

Tueckmantel, C., Fisher, Q.J., Grattoni, C.A. & Aplin, A.C. 2012. Single- and two-phase fluid flow properties of cataclastic fault rocks in porous sandstone. *Marine and Petroleum Geology*, **29**, 129 142, https://doi.org/10.1016/j.marpetgeo.2011.07.009

Turner, P., Burley, S.D., Rey, D. & Prosser, J. 1995. Burial history of the Penrith Sandstone (Lower Permian) deduced from the combined study of fluid inclusion and palaeomagnetic data. *In*: Turner, P. & Turner, A. (eds) *Palaeomagnetic Applications in Hydrocarbon Exploration and Production*. Geological Society, London, Special Publications, **98**, 43 78, https://doi.org/10.1144/gsl.sp.1995.098.01.04

Underhill, J.R., Gayer, R.A., Woodcock, N.H., Donnelly, R., Jolley, E.J. & Stimpson, I.G. 1988. The Dent Fault System, northern England reinterpreted as a major oblique-slip fault zone. *Journal of the Geological Society, London*, **145**, 303 316, https://doi.org/10.1144/gsjgs.145.2.0303

van Houten, F.B. 1973. Origin of red beds: A review 1961 1972. *Annual Review of Earth and Planetary Sciences*, **1**, 39 61, https://doi.org/10.1146/annurev.ea.01.050173.000351

Waugh, B. 1970*a*. Formation of quartz overgrowths in the Penrith Sandstone (Lower Permian) of Northwest England as revealed by scanning electron microscopy. *Sedimentology*, **14**, 309 320, https://doi.org/10.1111/j.1365-3091.1970.tb00197.x

Waugh, B. 1970*b*. Petrology, provenance and silica diagenesis of the Penrith Sandstone (Lower Permian) of Northwest England. *Journal of Sedimentary Petrology*, **40**, 1226 1240, https://doi.org/10.1306/74D72171-2B21-11D7-8648000102C1865D

Wennberg, O.P., Casini, G., Jahanpanah, A., Lapponi, F., Ineson, J., Wall, B.G. & Gillespie, P. 2013. Deformation bands in chalk, examples from the Shetland Group of the Oseberg Field, North Sea, Norway. *Journal of Structural Geology*, **56**, 103 117, https://doi.org/10.1016/j.jsg.2013.09.005

Wilson, M.D. 1992. Inherited grain-rimming clays in sandstones from eolian and shelf environments: Their origin and control on reservoir properties. *In*: Houseknecht, D.W. & Pittman, E.D. (eds) *Origin, Diagenesis, and Petrophysics of Clay Minerals in Sandstone*. SEPM Special Publications, **47**, 209 225, https://doi.org/10.2110/pec.92.47.0209

Worden, R.H. & Morad, S. 2002. Clay minerals in sandstones: controls on formation, distribution and evolution. *In*: Worden, R.H. & Morad, S. (eds) *Clay Mineral Cements in Sandstones*. Blackwell Science, Oxford, 3 42, https://doi.org/10.1002/9781444304336.ch1

Repository KITopen

Dies ist ein Postprint/begutachtetes Manuskript.

Empfohlene Zitierung:

Zitierung der Originalveröffentlichung: